

Frequency Domain Auto-tuning of Structured LPV Controllers for High-Precision Motion Control*

Yorick Broens, Hans Butler and Roland Tóth

Abstract—Motion systems are a vital part of many industrial processes. However, meeting the increasingly stringent demands of these systems, especially concerning precision and throughput, requires novel control design methods that can go beyond the capabilities of traditional solutions. Traditional control methods often struggle with the complexity and position-dependent effects inherent in modern motion systems, leading to compromises in performance and a laborious task of controller design. This paper addresses these challenges by introducing a novel structured feedback control auto-tuning approach for multiple-input multiple-output (MIMO) motion systems. By leveraging frequency response function (FRF) estimates and the linear-parameter-varying (LPV) control framework, the proposed approach automates the controller design, while providing local stability and performance guarantees. Key innovations include norm-based magnitude optimization of the sensitivity functions, an automated stability check through a novel extended factorized Nyquist criterion, a modular structured MIMO LPV controller parameterization, and a controller discretization approach which preserves the continuous-time (CT) controller parameterization. The proposed approach is validated through experiments using a state-of-the-art moving-magnet planar actuator prototype.

Index Terms—Mechatronics, LPV control, optimization.

I. INTRODUCTION

In recent years, there has been a significant focus on motion systems. These systems play a crucial role in enhancing the performance and reliability of various industrial processes and manufacturing systems, such as wafer scanners, industrial printers, pick-and-place machines and wire bonders, see [1]–[5]. Traditionally, motion control design for MIMO systems has leaned heavily on superior mechanical design principles, emphasizing factors such as high stiffness and reproducibility, see [6]. This approach has led to motion dynamics primarily characterized by rigid-body (RB) dynamics, facilitating the use of RB decoupling strategies to effectively mitigate low-frequency channel interaction, see [7]. In industrial settings, the integration of RB decoupling with sequential loop-closing (SLC) controller design is a common practice due to several practical advantages. Primarily, SLC facilitates the application of established loop-shaping techniques, see [8]. Moreover, it simplifies motion control design by relying on non-parametric

models, i.e. FRFs, thereby obviating the necessity for precise parametric system identification. Despite its advantages, the process of motion control design via SLC can present formidable challenges, particularly for high number of inputs and varying dynamics.

Modern motion systems often suffer from position-dependent effects, see [1]. These phenomena necessitate the adaptation of the RB decoupling technique to account for positional variations, thereby facilitating the implementation of SLC-based controller designs. Despite the effectiveness of this approach in achieving RB decoupling, often persistent high-frequency position-dependent couplings drive the SLC-based design to enforce robustness at the expense of performance degradation.

To automate motion control design in practise using FRF data only, various auto-tuning methods have been developed for SISO systems, see [9]–[12]. However, these approaches exhibit limitations in accommodating MIMO and position dependent dynamics. Alternatively, optimal gain controller synthesis techniques, such as robust \mathcal{H}_∞ and LPV \mathcal{L}_2 control, have emerged to provide efficient control design for MIMO dynamics even with position-dependent characteristics. Also, efficient tools for structured controller synthesis based on these approaches, i.e. using Hinfstruct, see [13], have been introduced. Nevertheless, the deployment of these latter approaches necessitate precise low-order parametric models capable of accurately capturing the high-frequency position-dependent channel interactions, which poses a formidable challenge in the context of modern system identification.

To overcome the gap between existing SISO approaches and required MIMO position dependent capabilities, this paper presents a novel frequency domain-based auto-tuning approach for LPV MIMO systems, relying solely on FRFs of the motion system, thus bypassing the need for complex parametric identification while providing local stability and performance guarantees.

In the extension of the current LTI auto-tuning schemes, the main contributions of this paper are:

- (C1) Development of a novel structured LPV MIMO feedback controller parameterization for auto-tuning, ensuring the modularity of controller design.
- (C2) Development of a MIMO stability check for both diagonal and full block controllers, relying only on FRF data.
- (C3) Development of a novel discrete-time LPV controller implementation, preserving the CT parameterization.

This paper is organized as follows. Section II presents the problem formulation, followed by the proposed structured feedback control parameterization in Section III. In Section IV, the optimization problem is introduced, encompassing an

*This work has received funding from the ECSEL Joint Undertaking (JU) programme under grant agreement No 875999 and from the European Union within the framework of the National Laboratory for Autonomous Systems (RRF-2.3.1-21.2022-00002).

Y. Broens, H. Butler and R. Tóth are with the Department of Electrical Engineering, Eindhoven University of Technology, Eindhoven, The Netherlands. H. Butler is also affiliated with ASML, Veldhoven, The Netherlands. R. Tóth is also affiliated with the Systems and Control Laboratory, HUN-REN Institute for Computer Science and Control, Hungary, (email: Y.L.C.Broens@tue.nl).

automated stability check and closed-loop performance shaping. Section V presents a controller implementation approach and experimental results of the frequency domain-based LPV MIMO structured feedback control auto-tuner on a state-of-the-art moving-magnet planar actuator (MMPA) prototype, while Section VI draws conclusions on the presented work.

II. PROBLEM FORMULATION

A. Background

Many modern motion systems exhibit position dependent effects due to their increasingly complex nature, see Figure 1. A common cause for this is the relative actuation and sensing of the moving-body, necessitating position dependent RB coordinate frame transformations to establish a relationship between the point of interest on the moving-body, the actuation forces and the actual position measurements. To accurately capture these effects, such systems are often represented in LPV form, where the position dependency is encapsulated within a scheduling vector, see [14]. Consider the equations of motion of a high-precision motion system that exhibits position dependent effects in the input and output:

$$M\ddot{x}(t) + D\dot{x}(t) + Kx(t) = G(p(t))f(t) \quad (1)$$

where M, D and $K \in \mathbb{R}^{n_x \times n_x}$ are the real symmetric mass, damping, and stiffness matrices and $G(p(t)) \in \mathbb{R}^{n_x \times n_f}$ maps the forces acting on the moving body, $f(t)$, to its center of gravity based on the scheduling vector $p(t) : \mathbb{R} \rightarrow \mathbb{P} \subseteq \mathbb{R}^{n_p}$. To allow for independent control of the mechanical degrees of freedom, (1) is typically represented in modal form, see [15]. This is achieved through a state transformation $x(t) = \tilde{V}\eta(t)$, where $\tilde{V} = M^{-\frac{1}{2}}V$. The eigenvector matrix V is derived from the characteristic dynamical equation $KV = MV\Lambda$, where Λ corresponds to the eigenvalue matrix. Grouping of the states per mode is achieved through a secondary state transformation $\eta(t) = T(\eta_{\text{RB}}^\top(t) \eta_{\text{FM}}^\top(t))^\top$ with:

$$T = (I_{n_x \times n_x} \otimes (1 \ 0)^\top \ I_{n_x \times n_x} \otimes (0 \ 1)^\top), \quad (2)$$

where \otimes corresponds to the *Kronecker-product*. Furthermore, the corresponding partitioned modal state-space representation of the motion system, denoted by \mathcal{P} , corresponds to:

$$\begin{pmatrix} \dot{\eta}_{\text{RB}}(t) \\ \dot{\eta}_{\text{FM}}(t) \\ y(t) \end{pmatrix} = \begin{pmatrix} A_{\text{RB}} & 0 & B_{\text{RB}}(p(t)) \\ 0 & A_{\text{FM}} & B_{\text{FM}}(p(t)) \\ \bar{C}_{\text{RB}}(p(t)) & \bar{C}_{\text{FM}}(p(t)) & 0 \end{pmatrix} \begin{pmatrix} \eta_{\text{RB}}(t) \\ \eta_{\text{FM}}(t) \\ f(t) \end{pmatrix}, \quad (3)$$

where $(\cdot)_{\text{RB}}$ are the system matrices that correspond to the rigid body modes and $(\cdot)_{\text{FM}}$ are the system matrices that coincide with the flexible modes. In the industry, motion control design for these type of systems is simplified through position dependent RB decoupling, which, in this case, is achieved by introducing the input and output decoupling matrices:

$$\begin{aligned} T_u &= \left((I_{n_{\text{RB}} \times n_{\text{RB}}} \otimes [0 \ 1]) B_{\text{RB}}(p(t)) \right)^\dagger \\ T_y &= \left(C_{\text{RB}}(p(t)) (I_{n_{\text{RB}} \times n_{\text{RB}}} \otimes [1 \ 0])^\top \right)^\dagger, \end{aligned} \quad (4)$$

where n_{RB} corresponds to the number of RB modes of the system. In this context, the RB decoupled system is given

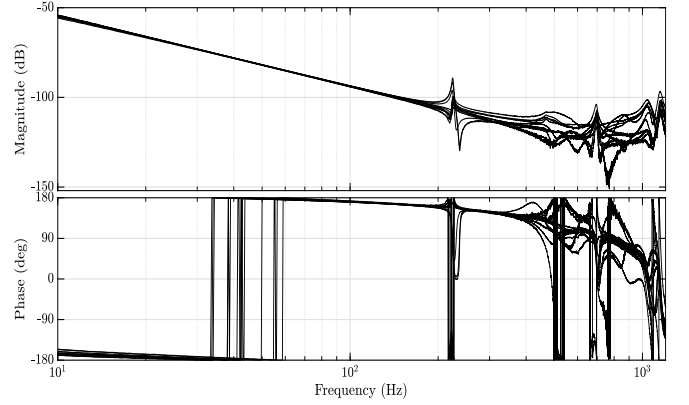


Fig. 1. Set of local frequency response functions of a high-precision moving-magnet planar actuator prototype, illustrating the high-frequency position dependent flexible dynamics for the RB decoupled transfer in R_y -direction.

by $\tilde{\mathcal{P}} = T_y \mathcal{P} T_u$. It is noteworthy to observe that introduction of the decoupling matrices results in an elimination of the position dependency in the RB dynamics, see Figure 1. Nonetheless, position dependent interaction still persists in the flexible dynamics, necessitating for robustified controller design at the cost of performance. An additional important observation is that in case the scheduling vector is constant, i.e. $p(t) = \mathbf{p}$ for all $t \in \mathbb{R}$, $\tilde{\mathcal{P}}$ becomes an LTI system, which is often referred to as *local dynamics* of the LPV system. For a given fixed \mathbf{p} , the *Fourier transform* of the local signal relation is given by:

$$Y(j\omega) = \tilde{\mathcal{P}}_{\mathbf{p}}(j\omega)U(j\omega), \quad (5)$$

where j is the imaginary unit, $\omega \in \mathbb{R}$ corresponds to the frequency and $\tilde{\mathcal{P}}_{\mathbf{p}}(j\omega)$ denotes the local frequency response function (IFRF) of $\tilde{\mathcal{P}}$. In this context, a set of IFRFs, denoted by $\{\tilde{\mathcal{P}}_i\}_{i=1}^n$, is obtained through closed-loop identification approaches for various forced equilibria of the system, i.e. around various operating points \mathbf{p} , thereby capturing the complex position dependent high-frequent effects in an accurate manner. Moreover, this set of IFRFs can be used for analyzing the local performance of a designated structured controller $\mathcal{K} \in \mathbb{R}^{n_{\text{RB}} \times n_{\text{RB}}}$ through the assessment of the magnitude constraints associated with closed-loop sensitivities across various frequency ranges. In this context, one may contemplate an optimization problem aimed at synthesizing structured controllers given a weighted plant. Similar to optimal gain-based control design, see [16], the construction of such a weighted plant is facilitated by shaping performance channels through frequency dependent filters.

B. Problem Statement

The problem that is being addressed in this paper is to develop a frequency-domain structured LPV MIMO feedback control auto-tuning approach by using IFRF measurements. We aim to accomplish this under the following requirements:

- (R1) The system is locally stabilized by \mathcal{K} for all $\mathbf{p} \in \mathbb{P}$.
- (R2) The control synthesis solely relies on IFRFs of the system, thus avoiding complex parametric identification.

III. CONTROLLER PARAMETERIZATION

This section introduces a novel modular LPV MIMO structured feedback controller parameterization for auto-tuning. To exploit the characteristics of typical motion systems, the structured feedback controller \mathcal{K} is divided into two main components as illustrated in Figure 2:

- (i) A low-frequency LTI controller, aimed at shaping the RB dynamics to achieve desired characteristics.
- (ii) A high-frequency LPV controller, designed to address position-dependent flexible dynamics.

To ensure modularity and scalability of the structured controller design, a novel structured parameterization approach is proposed, using *linear fractional representations* (LFRs). This approach involves extracting controller parameters into upper diagonal interconnections, resulting in diagonal parameter matrices to be optimized with respect to desired performance specifications, while the remainder of the dynamics of the controller is absorbed by the generalized plant for optimization.

A. Low-frequency LTI controller design

The control of RB modes conventionally employs a PID-type controller, see [16], which can be constructed by combining a PI-type controller with lead filters in a cascaded manner. It is worth noting that this controller configuration can also be implemented using a parallel controller structure. Nonetheless, the proposed controller parameterization accommodates both architectures as will be discussed in Subsection III-C. Consider the time-domain representation of a PI-controller:

$$\begin{aligned} \dot{x}_{\text{PI}}(t) &= u_{\text{PI}}(t) \\ y_{\text{PI}}(t) &= K_p x_{\text{PI}}(t) \end{aligned} \quad (6)$$

where $u_{\text{PI}}(t), y_{\text{PI}}(t) \in \mathbb{R}^{n_{\text{RB}}}$ correspond to the input and the output of the PI-controller and $K_p \in \mathbb{R}^{n_{\text{RB}} \times n_{\text{RB}}}$ is a diagonal matrix containing the proportional gains, ensuring that the local loop transfers, i.e. $\{\tilde{\mathcal{P}}_i \mathcal{K}_i\}_{i=1}^n$, cross the 0 dB line at the desired target bandwidths. To ensure closed-loop stability of the system, lead filters are often integrated alongside PI-controllers in a cascaded manner. The time-domain representation of a first order lead-filter is given by:

$$\begin{aligned} \dot{x}_{\text{LF}}(t) &= -\Omega_2 x_{\text{LF}}(t) + u_{\text{LF}}(t) \\ y_{\text{LF}}(t) &= (\Omega_1 - \Omega_2) x_{\text{LF}}(t) + u_{\text{LF}}(t) \end{aligned} \quad (7)$$

where $u_{\text{LF}}(t), y_{\text{LF}}(t) \in \mathbb{R}^{n_{\text{RB}}}$ correspond to the input and the output of the lead filter, and, $\Omega_1, \Omega_2 \in \mathbb{R}^{n_{\text{RB}} \times n_{\text{RB}}}$ are diagonal matrices containing the cut-off frequencies of the differentiations and integrators respectively. To accommodate sufficient phase lead at the target bandwidth, i.e. ± 45 degrees phase margin while being subject to the integral action of the PI controller, a third order lead filter is typically required.

B. High-frequency LPV controller design

To actively combat position dependent flexible dynamics, position dependent notch filters are employed. Consider the time-domain representation of a LPV notch filter:

$$\begin{aligned} \dot{x}_{\text{N}}(t) &= A_{\text{N}}(p(t))x_{\text{N}}(t) + B_{\text{N}}u_{\text{N}}(t) \\ y_{\text{N}}(t) &= C_{\text{N}}(p(t))x_{\text{N}}(t) + D_{\text{N}}u_{\text{N}}(t) \end{aligned} \quad (8)$$

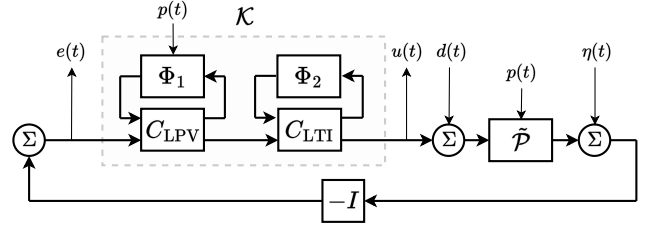


Fig. 2. Closed-loop motion control interconnection, where \mathcal{K} is partitioned into a low-frequency LTI controller and a high-frequency LPV controller.

where the state-space matrices are defined as follows:

$$\begin{aligned} A_{\text{N}}(p(t)) &= \begin{pmatrix} -2\beta_2(p(t))\omega_2(p(t)) & -\omega_2^2(p(t)) \\ I_{n_{\text{RB}} \times n_{\text{RB}}} & 0_{n_{\text{RB}} \times n_{\text{RB}}} \end{pmatrix} \\ B_{\text{N}} &= (I_{n_{\text{RB}} \times n_{\text{RB}}} \quad 0_{n_{\text{RB}} \times n_{\text{RB}}})^\top \\ C_{\text{N}}(p(t)) &= \begin{pmatrix} 2(\beta_1(p(t))\omega_1(p(t)) - \beta_2(p(t))\omega_2(p(t))) \\ \omega_1^2(p(t)) - \omega_2^2(p(t)) \end{pmatrix}^\top \\ D_{\text{N}} &= I_{n_{\text{RB}} \times n_{\text{RB}}} \end{aligned} \quad (9)$$

Here, $\beta_1(p(t)), \beta_2(p(t)) \in \mathbb{R}^{n_{\text{RB}} \times n_{\text{RB}}}$ represent diagonal matrices containing the damping ratios of the notch filter, which regulate the amplitude suppression at given notch frequencies $\omega_1(p(t)), \omega_2(p(t)) \in \mathbb{R}^{n_{\text{RB}} \times n_{\text{RB}}}$.

C. Controller interconnection

To allow for modularity and scalability of the controller design, the filters presented in (6), (7) and (8) are reformulated in an LFR form as illustrated in Figure 2. This is achieved by extracting the controller parameters into an upper diagonal interconnection, i.e. $\tilde{u}_i = \Phi_i \tilde{y}_i$, yielding the resulting LFR to be of form:

$$\begin{pmatrix} \tilde{y}_i(t) \\ y_i(t) \end{pmatrix} = \begin{pmatrix} P_{\tilde{y}_i \tilde{u}_i} & P_{\tilde{y}_i u_i} \\ P_{y_i \tilde{u}_i} & P_{y_i u_i} \end{pmatrix} \begin{pmatrix} \tilde{u}_i(t) \\ u_i(t) \end{pmatrix} \quad (10)$$

where $u_i(t), y_i(t) \in \mathbb{R}^{n_{\text{RB}}}$ correspond to the filter inputs and outputs and $\tilde{u}_i(t), \tilde{y}_i(t) \in \mathbb{R}^{n_{\text{par}}^i}$ are latent variables, describing the interconnections between the parameter blocks and the filter blocks, where n_{par}^i describes the number of filter parameters per specific filter $i \in [1, n_{\text{F}}]$. n_{F} represents the total number of filters considered during controller design. By reformulating individual controller components into LFR representation, a modular controller design approach is introduced, facilitating the derivation of diverse controller structures from two interconnection types: (i) cascade LFR interconnection and (ii) parallel LFR interconnection. Integration of these LFR representations yields a new LFR, with corresponding controller parameters consolidated into a diagonal matrix. Consequently, the closed-loop interconnection scheme, as depicted in Figure 2, is reformulated into a generalized plant description \mathfrak{P} , where LFR representations of controller filters are absorbed. As a result, the resulting diagonal generalized controller block $\mathfrak{K} = \text{diag}(\{\Phi_i\}_{i=1}^{n_{\text{F}}})$ exclusively encompasses controller parameters subject to optimization. Moreover, the presented structured controller parameterization affords both modularity and scalability in the design of controllers across

various structural configurations. This proposed controller parameterization is referenced as Contribution (C1) in this paper.

IV. AUTO-TUNING

This Section presents a novel frequency domain-based auto-tuning approach for structured LPV MIMO controllers based on the control interconnection illustrated in Figure 2. Consider the non-convex objective function:

$$\min_{\mathfrak{R}} \|\{M_i\}_{i=1}^n\|_{\mathcal{L}_\infty} + \Lambda_{\text{stab}}, \quad (11)$$

where $\{M_i\}_{i=1}^n$ denotes a collection of weighted generalized plants, and Λ_{stab} represents a stability constraint. Notably, the objective function seeks to minimize the \mathcal{L}_∞ -norm of the set of weighted plants through optimization of the parameter matrix \mathfrak{R} , while penalizing closed-loop stability through Λ_{stab} . It is important to note that in case closed-loop stability is ensured, the \mathcal{L}_∞ -norm corresponds to the \mathcal{H}_∞ -norm, i.e. local \mathcal{L}_2 -gain.

A. Stability Analysis

In this Subsection, an easy to check stability verification approach is presented which solely relies on IFRFs, in accordance with the principles of the Nyquist theorem, see [16]. Closed-loop stability is assessed through the set of local MIMO loop transfers:

$$\{L_i\}_{i=1}^n = \{\tilde{\mathcal{P}}_i \mathcal{K}_i\}_{i=1}^n, \quad (12)$$

The generalized Nyquist theorem employs Cauchy's argument principle as a pivotal mechanism to ascertain the count of closed-loop poles situated within the D -contour, which delineates a region in the complex plane, see [6]. It is important to note that in the context of MIMO systems, poles positioned along the imaginary axis are encompassed within the D -contour. Let P_{ol} denote the number of open-loop poles of $\{L_i\}_{i=1}^n$ that reside within the D -contour. Then, the system is closed-loop stable if and only if the image of $\{\det(I + L_i(j\omega))\}_{i=1}^n$ makes P_{ol} counterclockwise encirclements of the origin and does not pass through the origin as ω traverses the D -contour in clockwise direction. Note that the image of $\{\det(I + L_i(j\omega))\}_{i=1}^n$ can be constructed through IFRFs at the observed frequency points, allowing for the assessment of local closed-loop stability. However, analysis of the encirclements made by $\{\det(I + L_i(j\omega))\}_{i=1}^n$ presents a significant computational challenge. Specifically, the presence of the large number of integrators in MIMO systems, originating from RB modes and integral action of the structured feedback controller, results in the low-frequency behavior of the image exhibiting computationally unreliable characteristics, as the amplitude tends toward infinity. As a solution to this issue, a novel extension of the factorized Nyquist check is presented which decomposes the contour into a more computationally attractive alternative. Note that this is a generalization of the factorized Nyquist theorem, see [16], towards full block MIMO controllers. For a given local dynamics $\tilde{\mathcal{P}}_i$, consider the local MIMO interaction term E_i :

$$E_i = \left(\tilde{\mathcal{P}}_i \mathcal{K}_i - \hat{\mathcal{P}}_i \hat{\mathcal{K}}_i \right) \left(\hat{\mathcal{P}}_i \hat{\mathcal{K}}_i \right)^{-1}, \quad (13)$$

where \mathcal{K} is a full-block MIMO controller and:

$$\hat{\mathcal{P}}_i = \text{diag}(\{\tilde{\mathcal{P}}_i^{jj}\}_{j=1}^{n_{\text{RB}}}), \quad \hat{\mathcal{K}}_i = \text{diag}(\{\mathcal{K}_i^{jj}\}_{j=1}^{n_{\text{RB}}}), \quad (14)$$

which allows for decomposition of the Nyquist criterion as:

$$I + \tilde{\mathcal{P}}_i \mathcal{K}_i = (I + E_i \mathcal{T}_i) (I + \hat{\mathcal{P}}_i \hat{\mathcal{K}}_i), \quad (15)$$

where $\mathcal{T}_i = \tilde{\mathcal{P}}_i \hat{\mathcal{K}}_i (I + \hat{\mathcal{P}}_i \hat{\mathcal{K}}_i)^{-1}$. This reformulation results in a decomposition of the stability assessment as:

$$\det(I + L_i) = \det(I + E_i \mathcal{T}_i) \cdot \sum_{j=1}^{n_{\text{RB}}} \left(1 + \tilde{\mathcal{P}}_i^{jj} \mathcal{K}_i^{jj}\right) \quad (16)$$

From (16) it is observed that assessing the stability of $\det(I + L_i)$ is decomposed into $n_{\text{RB}} + 1$ encirclement checks, whereby the parts containing integrators are decoupled into SISO checks, ensuring the computational feasibility of the algorithm. The extended stability check for full block MIMO controllers based on IFRF data corresponds to Contribution (C2) of this letter.

B. Performance Shaping

In this Subsection, a norm-based performance optimization approach is presented, with particular reference to the set of weighted closed-loop IFRFs $\{M_i\}_{i=1}^n$ in (11). The non-convex nature of the cost function permits decomposition of the commonly employed 4-block shaping configuration, see [17], into four distinct shaping problems sharing common controller parameters. In this context, the performance channels, denoted by $w = (\eta \ d \ \eta \ d)^\top$ and $z = (e \ e \ u \ u)^\top$, see Figure 2, lead to the set of weighted closed-loop dynamics:

$$\{M\}_{i=1}^n = \left\{ W_z \cdot \text{diag} \left(\mathcal{S}_i, \mathcal{K}_i \mathcal{S}_i, \mathcal{S}_i \tilde{\mathcal{P}}_i, \mathcal{K}_i \mathcal{S}_i \tilde{\mathcal{P}}_i \right) \right\}_{i=1}^n \quad (17)$$

where $W_z = \text{diag}(W_z^S, W_z^{\mathcal{K}S}, W_z^{S\tilde{\mathcal{P}}}, W_z^{\mathcal{K}S\tilde{\mathcal{P}}})$ corresponds to an output shaping filter and $\{\mathcal{S}_i\}_{i=1}^n = \{(I + \tilde{\mathcal{P}}_i \mathcal{K}_i)^{-1}\}_{i=1}^n$. It is noteworthy that the partitioning of the shaping loops yields augmented flexibility in the design of W_z , given the decoupling of closed-loop sensitivities. To further capitalize on the non-convex characteristics of (11), the shaping filters are designed as piece-wise affine functions of frequency, thereby affording increased design flexibility compared to conventional frequency-domain based shaping filters. In this context, the sensitivity shaping filter W_z^S is designed to be of form:

$$W_z^S = K_s \cdot \text{diag} \left(\begin{cases} \frac{(\alpha^{-1} \omega_{\text{bw}}^i)^3}{\omega^3}, & \text{if } \omega \leq \frac{\omega_{\text{bw}}^i}{\alpha} \\ 1, & \text{else} \end{cases} \right), \quad (18)$$

where K_s is set to $0.5I$ to impose a 6dB upper-bound on the sensitivity, ω_{bw}^i corresponds to the target bandwidth of the i -th RB channel and $\alpha > 1$ is a tuning parameter that is used for sharpening of the sensitivity constraints. Similarly, the shaping filter for the complementary sensitivity $W_z^{\mathcal{K}S\tilde{\mathcal{P}}}$ is defined as:

$$W_z^{\mathcal{K}S\tilde{\mathcal{P}}} = K_r \cdot \text{diag} \left(\begin{cases} \frac{\omega}{\alpha \omega_{\text{bw}}^i}, & \text{if } \omega \geq \omega_{\text{bw}}^i \\ 1, & \text{else} \end{cases} \right), \quad (19)$$

where K_r is typically chosen as $0.5I$ to place a 6 dB upper-bound on the complementary sensitivity. The control sensitivity shaping filter $W_z^{\mathcal{K}S}$ is designed of the same structure

as (19). However, the design of K_r involves channel scaling, accomplished by setting $K_r = \text{diag}(\text{abs}(\mathcal{P}^{ii}(j\omega_{bw})))$ for all $i \in [1 n_{\text{RB}}]$. This selection corresponds to the worst-case gain concerning the modulus margin at the target bandwidth ω_{bw}^j , with an additional 6 dB margin applied on top of the filter. In a similar manner, the scaling of the process sensitivity is achieved by $K_p = \text{diag}(\text{abs}(\mathcal{P}^{ii}(j\omega_{bw}))^{-1})$, where the shaping filter for the process sensitivity W_z^{SP} corresponds to:

$$W_z^{SP} = K_p \cdot \text{diag} \left(\begin{cases} \frac{(\alpha^{-1}\omega_{bw}^j)}{\omega}, & \text{if } \omega \leq \frac{\omega_{bw}^j}{\alpha} \\ \frac{\omega}{\alpha\omega_{bw}^j}, & \text{if } \omega \geq \omega_{bw}^j\alpha \\ 1, & \text{else} \end{cases} \right) \quad (20)$$

C. Solving the optimization problem

To facilitate the auto-tuning of the structured LPV feedback controller, first, a desired feedback control structure must be specified according to the controller parameterization presented in Section III. Next, a set of weighted generalized plants is constructed by collapsing both the LFRs of the structured controller, and the desired shaping filters, e.g. (18), (19) and (20), into a weighted generalized plant representation of Figure 2. The resulting generalized controller \mathfrak{K} takes the form of a diagonal gain matrix comprising the controller parameters to be optimized. To optimize the non-convex cost function (11), we propose a two-step optimization strategy to converge towards a globally sub-optimal solution, aiming to minimize the \mathcal{H}_∞ -norm of the weighted plants $\{M_i\}_{i=1}^n$. This objective is achieved by penalizing closed-loop stability through the constraint Λ_{stab} , which is evaluated using (16). If the closed-loop is stable, Λ_{stab} is excluded from the cost function; however, in the case of instability, Λ_{stab} is assigned a high-cost penalty, thereby penalizing the overall cost function. The optimization process is initiated with particle swarm optimization (PSO), a stochastic optimization algorithm well-regarded for its ability to explore the global search space for optimal parameters, see [18]. Nevertheless, due to PSO's indiscriminate exploration, it may not guarantee the discovery of either a global or local optimum. Consequently, a secondary optimization step is introduced, employing gradient-descent methodologies, particularly the BFGS optimization technique, see [19]. This step is initialized with the PSO-based solution, thereby improving overall cost optimization by converging towards a local minimum, therefore satisfying (R1) and (R2).

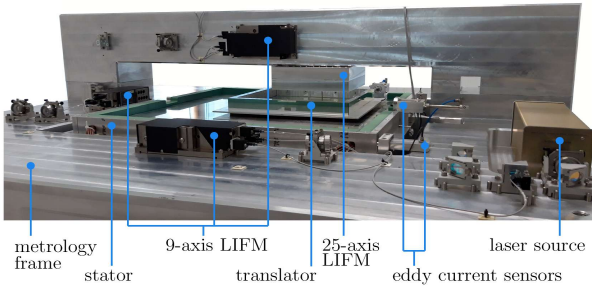


Fig. 3. Photograph of a moving-magnet planar actuator system prototype.

V. EXPERIMENTAL VALIDATION

A. MMPA Prototype System

A MMPA system, illustrated in Figure 3, displays position-dependent effects due relative actuation and sensing of the moving-body. Comprising three key components, this system includes a stator base housing a double-layer coil array, a lightweight translator equipped with a Hallbach array consisting of 281 permanent magnets, and a metrology frame featuring 9 laser interferometers for precise displacement measurement of the translator. For a comprehensive overview of such a prototype, refer to [20].

B. Controller implementation

In this Subsection, a novel discretization approach is introduced that maintains the parameterization of CT controllers, preserving their physical interpretation in the resulting discrete-time (DT) domain. Leveraging the modularity of the structured controller design outlined in Section III, the LFR representation of the controller is discretized. The resulting DT controller is obtained by collapsing back the CT parameters obtained from auto-tuning. Moreover, consider the CT state-space representation of (10):

$$I s^{-1} \star \begin{pmatrix} A_i & B_i \\ C_i & D_i \end{pmatrix}, \quad (21)$$

where s corresponds to the *Laplace operator* and \star is the *star product*. Note that in the time-domain, s^{-1} is replaced by an integrator. To maintain the CT parameterization of the controller, our objective is to articulate the discretization utilizing a time-domain operator, as opposed to employing matrix operations to transform the state-space realization to the z -domain. In [21], a frequency domain discretization technique has been introduced capable of retaining the CT parameterization through a so called w '-domain transformation:

$$w' = \frac{2}{T_s} \frac{s-1}{s+1}, \quad (22)$$

where T_s is the sampling time. In this context, we introduce a time-domain equivalent of (22) in terms of an r -operator:

$$r(q) := \left(\begin{array}{c|c} -I & \frac{4}{T_s} I \\ \hline -I & \frac{2}{T_s} I \end{array} \right) \quad (23)$$

where q corresponds to the time shift operator. Substitution of the r -operator with the integrators in the time-domain results in the DT-representation of (10):

$$I r^{-1}(q) \star \begin{pmatrix} A_i & B_i \\ C_i & D_i \end{pmatrix}, \quad (24)$$

where $r^{-1}(q)$ corresponds to:

$$r^{-1}(q) := \left(\begin{array}{c|c} I & 2I \\ \hline \frac{T_s}{2} I & \frac{T_s}{2} I \end{array} \right) \quad (25)$$

The interconnection of (24) is well-posed if and only if $\det(I - A_i \frac{T_s}{2}) \neq 0$, which is automatically satisfied due to the LFR form of the controller. Additionally, note that the r^{-1} operator can be directly integrated in the optimization

of the CT controller parameters using (11), allowing for direct DT controller synthesis using the CT parameterization. Nonetheless, this adjustment necessitates adaption of the stability analysis, as encirclements must now be considered along the C -contour. The presented DT controller implementation corresponds to Contribution (C3) in the paper.

C. Experimental Results

To showcase the effectiveness of the structured feedback control auto-tuning approach, two types of MIMO controllers were synthesized employing the methodology detailed in Section IV. Each controller configuration comprises a PI-controller described by equation (6), augmented by three lead filters of the form (7), and a notch filter of form (8). It is noteworthy that for the robust controller, the notch filter is designed invariant of position, while for the LPV controller, the notch coefficients are assumed to exhibit a first-order polynomial dependence on the scheduling vector. Synthesis of both controllers utilized 11 IFRFs of the MMPA prototype via the shaping approach outlined in Subsection IV-B.

To experimentally validate the efficacy of these controllers, lithographic scanning motions were performed, see [1], in both the x and y directions simultaneously, employing a fourth-order motion profile, with $a_{\max} = 10 \frac{m}{s^2}$, $v_{\max} = 0.2 \frac{m}{s}$, and maximum displacement in both x and y direction of $0.05m$.

The experimental results, depicted in Figure 4, were acquired under identical operational conditions. The blue graph represents the position tracking error in the R_y direction using the robust controller, while the red graph illustrates the position tracking error in the R_y direction employing the LPV controller. The selection of the R_y axis is motivated by its significant limitation due to the presence of position-dependent flexible dynamics, as depicted in Figure 1. Analysis of the results presented in Figure 4 yields several conclusions. Firstly, it is evident that the LPV controller outperforms the robust controller. Notably, during the scanning interval, the worst-case error is reduced from 11.55×10^{-6} rad to 6.78×10^{-6} radians, signifying a relative improvement of 43.10% in performance. This improvement can be attributed to the additional degree of freedom provided by the position dependency of the notch filter during controller synthesis.

VI. CONCLUSION

This paper introduces a novel frequency domain auto-tuning technique tailored for structured LPV MIMO controllers, leveraging solely frequency domain data. The presented methodology introduces an innovative controller parameterization scheme, enabling modular structured controller synthesis. Experimental validation carried out on a MMPA prototype demonstrates the effectiveness of the proposed approach, where both robust and LPV MIMO controllers were synthesized. The LPV controller achieves a relative performance improvement of 43.10% in the R_y -direction compared to the synthesized robust controller.

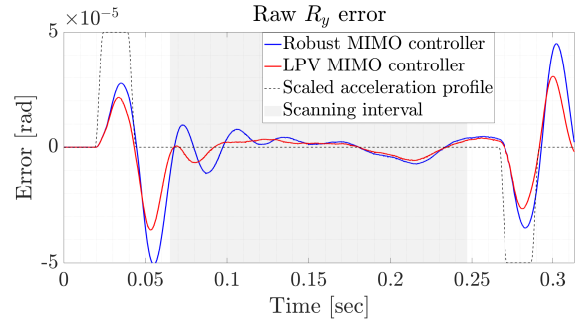


Fig. 4. Position tracking error in R_y direction during the constant velocity interval of the motion profile with: (—) Robust controller, (—) LPV controller.

REFERENCES

- [1] H. Butler, "Position control in lithographic equipment: Applications of control," *IEEE Control Systems Magazine*, no. 5, pp. 28–47, 2011.
- [2] K. Ohnishi, et al., "Motion control for advanced mechatronics," *IEEE/ASME Trans. on Mech.*, vol. 1, no. 1, pp. 56–67, 1996.
- [3] B. Bukkems, R. van de Molengraft, M. Heemels, N. van de Wouw, and M. Steinbuch, "A piecewise linear approach towards sheet control in a printer paper path," in *Proc. Amer. Control Conf. (ACC)*, 2006.
- [4] T. Qu, J. Chen, S. Shen, Z. Xiao, Z. Yue, and H. Y. Lau, "Motion control of a bio-inspired wire-driven multi-backbone continuum minimally invasive surgical manipulator," in *Proc. of the IEEE International Conference on Robotics and Biomimetics*, pp. 1989–1995, 2016.
- [5] X. Ye, Y. Zhang, and Y. Sun, "Robotic pick-place of nanowires for electromechanical characterization," in *Proc. of the 2012 IEEE International Conference on Robotics and Automation*, pp. 2755–2760, 2012.
- [6] T. Oomen, "Advanced motion control for precision mechatronics: control, identification, and learning of complex systems," *IEEE Journal of Industry Applications*, vol. 7, no. 2, pp. 127–140, 2018.
- [7] M. Steinbuch, "Design and control of high tech systems," in *Proc. of the IEEE international Conference on Mechatronics*, pp. 13–17, 2013.
- [8] M. Steinbuch and M. Norg, "Advanced motion control: An industrial perspective," *European Journal of Control*, pp. 278–293, 1998.
- [9] X.-j. Zhu et al., "A simple auto-tuner in frequency domain," *Computers & chemical engineering*, vol. 30, no. 4, pp. 581–586, 2006.
- [10] E. van Solingen, J. van Wingerden, and T. Oomen, "Frequency-domain optimization of fixed-structure controllers," *International Journal of Robust and Nonlinear Control*, vol. 28, no. 12, pp. 3784–3805, 2018.
- [11] C. Hwang and C.-Y. Hsiao, "Solution of a non-convex optimization arising in pi/pid control design," *Automatica*, vol. 38, no. 11, pp. 1895–1904, 2002.
- [12] H. Panagopoulos, K. Astrom, and T. Hagglund, "Design of pid controllers based on constrained optimization," in *Proc. Amer. Control Conf. (ACC)*, vol. 6, pp. 3858–3862, IEEE, 1999.
- [13] P. Gahinet and P. Apkarian, "Decentralized and fixed-structure H_∞ control in MATLAB," in *2011 50th IEEE conference on decision and control and european control conference*, pp. 8205–8210, IEEE, 2011.
- [14] R. Toth, H. S. Abbas, and H. Werner, "On the state-space realization of lpv input-output models: Practical approaches," *IEEE Transactions on Control Systems Technology*, vol. 20, no. 1, pp. 139–153, 2012.
- [15] W. K. Gawronski, *Dynamics and control of structures: A modal approach*. Springer Science & Business Media, 2004.
- [16] S. Skogestad and I. Postlethwaite, *Multivariable feedback control: analysis and design*. 2007.
- [17] M. Van de Wal, G. van Baars, F. Sperling, and O. Bosgra, "Multivariable H_∞/μ feedback control design for high-precision wafer stage motion," *Control engineering practice*, vol. 10, no. 7, pp. 739–755, 2002.
- [18] R. Eberhart and J. Kennedy, "Particle swarm optimization," in *Proc. IEEE Int. Conf. on neural networks*, vol. 4, pp. 1942–1948, 1995.
- [19] R. Battiti and F. Masulli, "BFGS optimization for faster and automated supervised learning," in *Proc. Int. Neural Network Conf.*, pp. 757–760, Springer, 1990.
- [20] I. Proimadis et al., "Active deformation control for a magnetically levitated planar motor mover," *IEEE Transactions on Industry Applications*, vol. 58, no. 1, pp. 242–249, 2021.
- [21] R. Whitbeck and L. Hofmann, "Digital control law synthesis in the w'domain," *J. of Guid. and Control*, vol. 1, no. 5, pp. 319–326, 1978.